AGU PUBLICATIONS

JGR

Journal of Geophysical Research: Oceans

RESEARCH ARTICLE

10.1002/2017JC012808

Persistent Shoreline Shape Induced From Offshore Geologic Framework: Effects of Shoreface Connected Ridges

Ilgar Safak[1], Jeffrey H. List[1], John C. Warner[1], and William C. Schwab[1]

[1]United States Geological Survey, Coastal and Marine Science Center, Woods Hole, MA, USA

Key Points:
- Persistent shoreline shape linked to effect of shelf geologic framework on nearshore sediment fluxes
- Cross-shore flows between shelf and nearshore are important in decadal scale coastal evolution
- Shoreline shape controlled by ridge effects on wave breaking, vortex force, advection, pressure gradient

Correspondence to:
I. Safak,
isafak@usgs.gov

Citation:
Safak, I., List, J. H., Warner, J. C., & Schwab, W. C. (2017). Persistent shoreline shape induced from offshore geologic framework: Effects of shoreface connected ridges. *Journal of Geophysical Research: Oceans*, *122*, 8721–8738. https://doi.org/10.1002/2017JC012808

Received 20 FEB 2017
Accepted 10 OCT 2017
Accepted article online 15 OCT 2017
Published online 15 NOV 2017

Abstract Mechanisms relating offshore geologic framework to shoreline evolution are determined through geologic investigations, oceanographic deployments, and numerical modeling. Analysis of shoreline positions from the past 50 years along Fire Island, New York, a 50 km long barrier island, demonstrates a persistent undulating shape along the western half of the island. The shelf offshore of these persistent undulations is characterized with shoreface-connected sand ridges (SFCR) of a similar alongshore length scale, leading to a hypothesis that the ridges control the shoreline shape through the modification of flow. To evaluate this, a hydrodynamic model was configured to start with the US East Coast and scale down to resolve the Fire Island nearshore. The model was validated using observations along western Fire Island and buoy data, and used to compute waves, currents and sediment fluxes. To isolate the influence of the SFCR on the generation of the persistent shoreline shape, simulations were performed with a linearized nearshore bathymetry to remove alongshore transport gradients associated with shoreline shape. The model accurately predicts the scale and variation of the alongshore transport that would generate the persistent shoreline undulations. In one location, however, the ridge crest connects to the nearshore and leads to an offshore-directed transport that produces a difference in the shoreline shape. This qualitatively supports the hypothesized effect of cross-shore fluxes on coastal evolution. Alongshore flows in the nearshore during a representative storm are driven by wave breaking, vortex force, advection and pressure gradient, all of which are affected by the SFCR.

1. Introduction

The horizontal and vertical structure, composition and distribution of sediment on the seabed are characterized by the geologic framework of the inner continental shelf and coastal zone. This framework has been hypothesized to impose a strong influence on nearshore oceanographic processes and coastal evolution (e.g., Denny et al., 2013; Houser et al., 2008; Riggs et al., 1995; Schupp et al., 2006; Schwab et al., 2000; Wright et al., 1991). These effects can occur on various length and time scales through both the effects of offshore bathymetric features on wave- and current-induced flow patterns in the nearshore and also possible cross-shore exchange of sediment between the nearshore and the inner-shelf. Examples of where the geologic framework is strongly varying spatially are the inner shelves of Mississippi (Flocks et al., 2015), West Florida (Finkl et al., 2007), South Carolina (Denny et al., 2013), Delmarva Peninsula (Pendleton et al., 2015), and New York (Schwab et al., 2013). Such inner-shelf areas have rarely been mapped in high resolution. In this study, effects of geologic framework on coastal evolution are investigated in Fire Island, located along the southern shore of Long Island, New York, USA (Figure 1).

1.1. Study Site: Fire Island

Fire Island is a 50 km long barrier island with many and sometimes conflicting land uses, such as national and state parks, coastal communities, and wilderness areas. The island is oriented roughly along WSW-ENE direction, and is bounded between the Fire Island Inlet at the west and the Moriches Inlet at the east (Figure 1). Offshore of the eastern half of the island between km 30 and km 50 (distances measured eastward from Fire Island Inlet; Figure 1), isobaths on the seafloor bathymetry are considerably parallel to the shore. In contrast, the inner continental shelf offshore of the western half of the island (km 1–25) is characterized with a series of shoreface connected sand ridges (SFCR) that are several meters thick, 5–10 km long and oriented obliquely to the coastline and spaced several kilometers apart. The source of sediment for these features is the erosion of the glacial outwash lobe located near the center of the island near km 25–

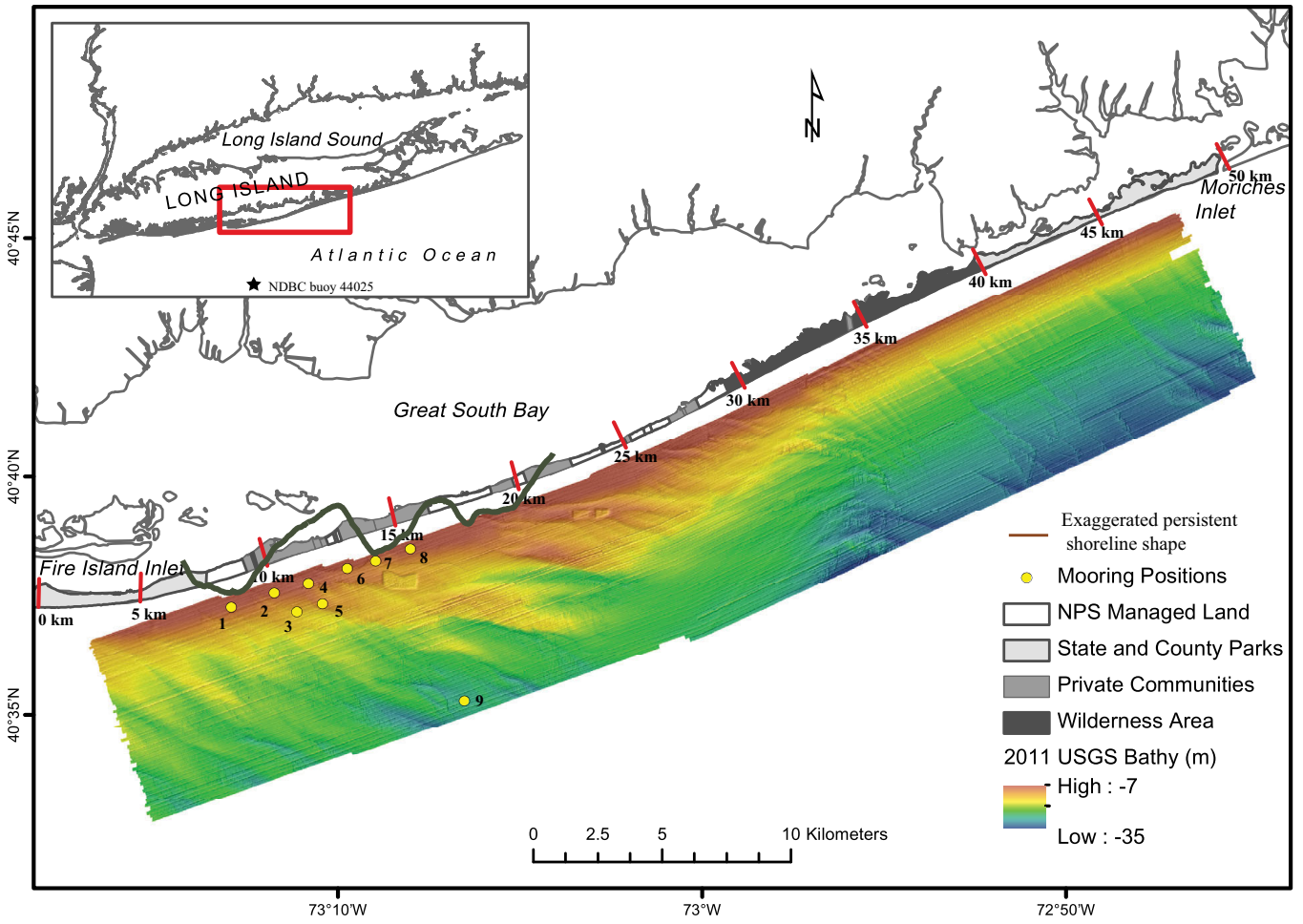

Figure 1. Map and inner-shelf bathymetry (in m) of Fire Island, New York, USA (modified from Schwab et al. [2013] and Lentz et al. [2013]). Numbers along the island indicate the alongshore distance from the Fire Island Inlet at the west to the Moriches Inlet at the east. Numbered circles on the bathymetry indicate the instrumentation platform locations in the 2014 Experiment. The heavy green curve between km-7 and km-22 delineates the persistent undulations on the shoreline (i.e., the average shoreline position between 1962 and 2012) exaggerated in the cross-shore direction. Dredged areas (borrow pits) are seen about 2-km offshore of km-15 and km-22.

30 (Schwab et al., 2000), however, oceanographic processes form and maintain the SFCR (Liste et al., 2016; Warner et al., 2014). Oceanographic and geologic investigations along Fire Island have focused on the aspects of SFCR maintenance (Warner et al., 2014) and SFCR effects on evolution of Fire Island coast (Kana et al., 2011; Lentz et al., 2013; List et al., 2016; Rosati et al., 1999; Schwab et al., 2013, 2014; Swift et al., 1985). Fire Island has recently been subject to increasing attention also due to the impact of Hurricane Sandy in October 2012 (Goff et al., 2015; Schwab et al., 2017; Warner et al., 2017) which identified the need to further understand the variations of impacts from storm events.

Coastal evolution and shoreline positions along Fire Island have been investigated previously. Allen and LaBash (1997) showed that the decadal shoreline change along the western half of Fire Island has longer cross-shore and alongshore length scales as compared to the eastern half (reproduced here in Figure 12). However, that study did not identify connections between shoreline response and the adjacent features on the inner-shelf such as the SFCR. Schwab et al. (2000) speculated that the shoreline response reported by Allen and LaBash (1997) could be due to wave shoaling over the adjacent SFCR and wave focusing on certain parts of the shoreline at an alongshore length scale related to the ridge geometry and the alongshore spacing of the adjacent ridges. However, the physical processes that might link the SFCR to shoreline evolution have not been directly investigated or explained, and are the focus of this study. Here we hypothesize that the shoreline along the western segment of Fire Island maintains a long-term persistent undulating shape that is controlled by the effects of the adjacent SFCR on the nearshore flow and sediment transport

processes. To investigate this hypothesis, first, a comprehensive shoreline position data set along Fire Island that covers the last 50 years is analyzed to evaluate shoreline positions and shoreline change rates. Then, a hydrodynamics-based open-source model that couples a wave model, an ocean circulation model, and a sediment transport model is applied to compute suspended load and bedload fluxes in the coastal region along Fire Island. The model is first evaluated using a comprehensive field data set collected along and across the SFCR field offshore of Fire Island, and historical observations from nearby buoys. Then, additional numerical experiments are conducted to compute sediment fluxes and investigate the physical processes linking the SFCR to the long-term shoreline shape. The model results are analyzed and discussed together with the shoreline shape observations. Contributions of cross-shore flows on the observed decadal-scale shoreline shape are evaluated.

2. Shoreline-Based Analysis

The coastal response along Fire Island is analyzed using a data set of 35 shoreline positions collected between 1962 and 2012 (Hapke et al., 2010). The data become more frequent after 1993 and contain one shoreline position for almost every year between 1993 and 2012. The earlier data were derived from aerial photographs and, starting in early 1990s, from ground-based GPS surveys and airborne LIDAR surveys. The shoreline database includes a mixture of the visually interpreted High Water Line (HWL) and datum-based Mean High Water (MHW) shorelines, requiring a "proxy-datum bias" correction to remove the bias between these two measures of shoreline position (Ruggiero & List, 2009).

All locations along Fire Island have approximately 50–100 m of shoreline position variability in the cross-shore over the 50 years analyzed here (Figure 2a). However, along the western section of the island (between km 7–16, highlighted with dark brown in Figures 1 and 2b), the shoreline tends to exhibit a persistent undulating shape with alongshore length scales of 3–4 km and cross-shore amplitudes of 20–40 m. One possible mechanism for the formation of shoreline undulations of these alongshore length scales has been proposed to be the instability due to high-angle, oblique waves (Ashton et al., 2001; Falques et al., 2017; Kaergaard et al., 2012). This undulating shape along the western section of the island can be represented by the 1962–2012 average shoreline position, which is superimposed on the position of all 35 shorelines in Figure 2a. In other areas of Fire Island, especially eastward of km 30, the shoreline shape is more variable through time without a persistent shape (not shown). The section of the coast with a persistent undulating shape, i.e., the persistent undulation zone, lies onshore of the SFCR (Figures 1 and 2b), while the inner-shelf is relatively uniform offshore of the eastern half of the island where no persistent shoreline shape is observed. These observations form the basis for the hypothesis we are testing here, i.e., the persistent shoreline shape is controlled by the prominent inner-shelf ridges and troughs located offshore in this area (Figure 1).

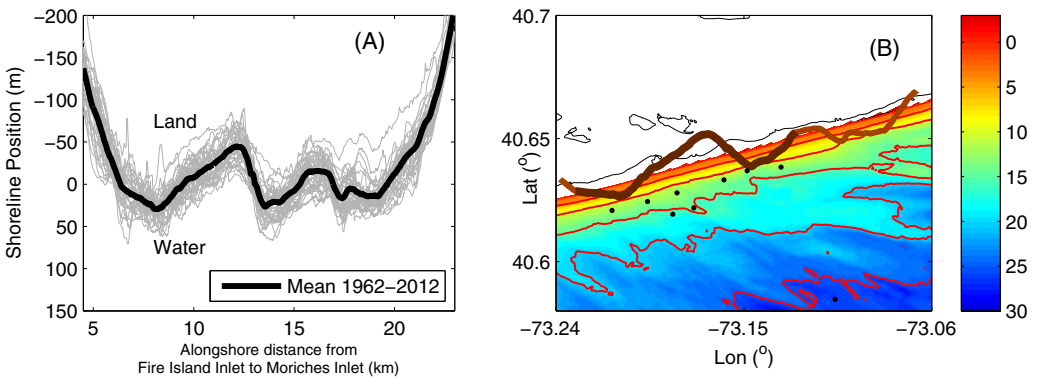

Figure 2. Persistent undulations at the shoreline of Fire Island: (a) measured shoreline positions as a function of the distance along the reference line in Figure 1 (thick black curve shows the mean of the shoreline positions); (b) Thick brown curve shows the cross-shore exaggerated mean shoreline position within the persistent undulation zone (darker brown highlights the part of the undulations where the persistence is higher) on the bathymetry (in m). On (b), thin black curve delineates the shoreline; red curves on the bathymetry correspond to the 5, 10, 15, 20, and 25 m isobaths; black dots indicate the locations of the instrumentation platforms and buoys during the 2014 Experiment.

The primary model prediction here is the alongshore variation of the long-term net alongshore transport (see section 3) which is a major control in barrier island evolution (Safak et al., 2016). Therefore, a quantitative method of comparing the observed average shoreline shape to this prediction is required. Assuming the generation of the undulating shoreline shape from an initially straight coast, the number of years this would take and translate the shoreline shape into a shoreline change rate curve (as function of distance alongshore) is assumed. Then the shoreline continuity equation is used to estimate the alongshore variations in alongshore transport that would be required if this shoreline change rate was entirely the result of this process. This is essentially the transport derived from observed shoreline change in an inverse manner, i.e., shoreline-derived transport. The shoreline continuity equation relates the shoreline change rate to transport gradients as:

$$\frac{\partial x}{\partial t} = -\frac{1}{h}\frac{\partial Q}{\partial y}, \tag{1}$$

where $x(y, t)$ is the shoreline position, t is time, h is an assumed depth to which bathymetric contours shift laterally at the same rate as the shoreline (viz, the "closure depth"), Q is the net cross-shore integrated alongshore sediment transport flux, and y is the alongshore dimension. Discretizing equation (1) and solving for the transport into (Q_{in}) and out of (Q_{out}) each discretized cell give:

$$Q_{out} = Q_{in} - h\frac{\Delta x}{\Delta t}\Delta y. \tag{2}$$

This formulation needs a boundary condition on the upstream end. Here, Q_{in} is set near the updrift (east) boundary as the model-predicted transport to facilitate a visual comparison between model-predicted and shoreline-derived transport curves. It is important to note that the choice of Q_{in} only shifts the entire shoreline-based transport curve by a constant factor, and does not affect the results or conclusions presented here.

The closure depth, h, in equations (1) and (2), can be viewed as the depth to which a change in nearshore and shoreface sediment volume (as resulting from an alongshore transport gradient) would, on long time scales (order of decades), be reflected in a translation of the shoreline position. Schwab et al. (2014) used geophysical data to quantify the depth of the "modern beach wedge" or the modern sediments associated with the subaerial beach. These "toe depths" ranged from about 10 to 17 m along Fire Island with an average depth of 13.8 m. The shoreline-derived alongshore transport computed from equation (2) was found to have little sensitivity to h in this range and we simply used this average toe depth here.

The model-generated and shoreline-derived transport curves can be quantitatively compared by differencing the alongshore gradients of the two curves to give a "sediment flux residual" or the component of the observed shoreline shape that cannot be explained by modeled alongshore transport gradients (because only the gradients are compared, the results are unaffected by the choice of Q_{in}). The flux residual, in units of m^3/yr per alongshore meter of coast, can be viewed as the volume of sediment needed to close the sediment budget within each cell, i.e., the cell's sediment volume change that cannot be explained by (modeled) alongshore variations in transport.

The assumed number of years for generating the persistent shoreline undulation shape from an (imaginary) initially straight coast was set to 30 years to minimize the sediment flux residual, i.e., maximize the correspondence between the shoreline-derived and model-simulated transport gradients. Note that the number of years cannot be selected to force a match in the pattern of shoreline-derived and model-predicted transport variations, but can only scale the magnitude of the shoreline-derived transport variations. The value of 30 years selected here has little meaning, as obviously there was no initial straight coast (at least within our observation period). However, it indicates that it is a decadal scale process for the model-predicted transport gradients to generate the persistent undulating shoreline shape from a straight coast, assuming a closure depth of 13.8 m.

3. Modeling

3.1. Model Physics and Setup

In this study, the Coupled Ocean-Atmosphere-Wave-Sediment Transport modeling system (COAWST) is used for modeling the three-dimensional hydrodynamic, wave, and sediment transport processes (Warner

et al., 2010). The COAWST modeling system couples the Regional Ocean Modeling System (ROMS) with a spectral wave model (SWAN) and contains suspended sediment and bedload transport algorithms. The model coupling provides exchanges of data fields between the modeling components. ROMS provides water levels and current velocities to SWAN; SWAN exchanges wave parameters of wave height, length, period and orbital velocities to ROMS. This allows the wave-induced effects on mean currents to be accounted for in the integration of the momentum equations using the vortex force formalism. The depth-averaged alongshore momentum balance, investigated in detail in section 5.3, is:

$$D\frac{\partial \bar{v}}{\partial t}+D\left[\frac{\partial(\bar{u}\bar{v})}{\partial x}+\frac{\partial(\bar{v}\bar{v})}{\partial y}+\bar{v}\frac{\partial \overline{u^{st}}}{\partial x}+\bar{v}\frac{\partial \overline{v^{st}}}{\partial y}\right]+Df\left(\bar{u}+\overline{u^{st}}\right)=D\overline{F^{wy}}-D\frac{\partial \bar{\phi}}{\partial y}-D\overline{u^{st}}\left(\frac{\partial \bar{v}}{\partial x}-\frac{\partial \bar{u}}{\partial y}\right)+\frac{\tau_{sy}}{\rho}-\frac{\tau_{by}}{\rho}, \quad (3)$$

where D is total water depth, $\bar{u}$ and $\bar{v}$ are the vertically averaged Eulerian mean velocities in the cross-shore and alongshore directions, respectively, $\overline{u^{st}}$ and $\overline{v^{st}}$ are the vertically integrated Stokes velocities in the cross-shore and alongshore directions, respectively, f is the Coriolis parameter, F^{w} is the momentum flux from nonconservative wave terms, ϕ is the geopotential function, τ_s is the surface stress, τ_b is the bottom stress, and ρ is the water density. The terms on the left-hand side are local acceleration, horizontal advection and the Coriolis force, respectively. The terms on the right-hand side are nonconservative wave forcing (wave breaking), pressure gradient, horizontal vortex force, surface stress and bottom stress, respectively. Effects of wave-current interaction on the bottom boundary layer processes and on sediment transport are also parameterized in COAWST. For further details on the modeling system such as numerical schemes, coupling methods, wave-current interaction, sediment transport algorithms and model validation, the reader is referred to Warner et al. (2008a, 2008b, 2010); Kumar et al. (2012), and references therein.

Major sources of nearshore and inner-shelf bathymetry used for the model grids are from high resolution mapping of the area in 2011 by the United States Geological Survey (Schwab et al., 2013) and the LIDAR data collected right before Hurricane Sandy in October 2012 (http://coastal.er.usgs.gov/hurricanes/sandy/lidar/). Where necessary, additional bathymetry was used such as from the NOAA Coastal Relief Model and ETOPO-2 bathymetry data sets. All the bathymetry was merged into a common datum and smoothed to provide a coherent consistent data surface.

The modeling approach utilizes a quadruple-nested grid setup (Figure 3) to start from a large domain that encompasses oceanographic processes, allows to account for the effects of waves of all periods, origins, directionalities, and obliquity (therefore, not only locally generated waves) and scales down to resolve detailed coastal flows. The largest outermost grid starts with the 5 km resolution USEast grid (896 $\times$ 336 cells), spans along the coastline of the US East Coast (Figure 3a), includes the Gulf of Mexico and has been used for daily forecast (http://woodshole.er.usgs.gov/project-pages/cccp/public/COAWST.htm). This grid provides boundary forcing to the New York Bight grid with 700 m resolution and 345 $\times$ 107 cells (Figure 3b). The third grid in the model setup is the 100 m resolution Fire Island Shelf grid with 765 $\times$ 170 cells (Figure 3c). Finally, the nearshore strip grid is nested into the Shelf grid; this strip grid is composed of 1,280 $\times$ 214 cells and has a resolution of 5–40 m with higher resolution in the shallow areas and the surf zone (Figure 3d).

Surface wave fields were modeled with SWAN on all four rectangular grids and used a time stepping of Δt=2.5 min on the strip grid and 5 min on the coarser three grids. ROMS was run with a time step of Δt=3 s and coupled with SWAN on the nearshore strip grid. Data fields were exchanged every hour in order to compute the waves, circulation and resulting sediment fluxes. ROMS was simulated to have 10 vertical levels, and a zero-gradient boundary condition for the free-surface, depth-averaged and baroclinic velocities at the open boundaries. All four grids were forced with winds from the hindcasts of North American Regional Reanalysis (NARR; ftp://ftp.cdc.noaa.gov/Datasets/NARR/monolevel/), and North American Mesoscale Model where available, for SWAN and ROMS. USEast grid, in addition, was forced with WaveWatch III hindcasts of NCEP (Chawla et al., 2013) for its lateral boundary conditions for surface waves. Suspended sediment and bedload transport algorithms (Warner et al., 2008a) were used for computing sediment fluxes. Results in the related parts in the following sections are presented as alongshore sediment fluxes integrated in the cross-shore starting from the coast up to 13.8 m depth which is the mean shoreface toe depth observed offshore of Fire Island (section 2; Schwab et al., 2014). To investigate the sensitivity of the results on the depth range of cross-shore integration, alongshore sediment fluxes were integrated in the cross-shore starting from the coast up to 8 m depth as well, which is onshore of the SFCR field and offshore of

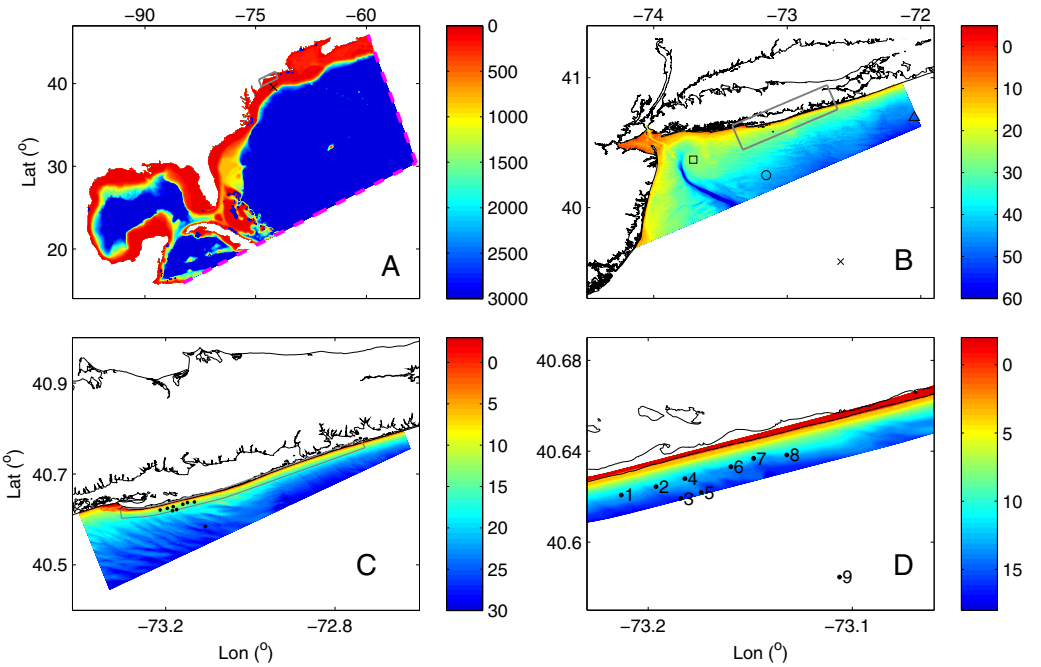

Figure 3. Model grid setup and bathymetries (in m): (a) 5 km resolution USEast grid (dashed magenta lines indicate where the wave boundary conditions are set based on the global wave model WaveWatch III; the gray rectangle shows the extent of the 700 m resolution New York Bight grid); (b) 700 m resolution New York Bight grid (the gray rectangle shows the extent of the 100 m resolution Fire Island Shelf grid); (c) 100 m resolution Fire Island Shelf grid (the gray polygon shows the extent of the 5–40 m resolution Fire Island Strip grid); (d) 5–40 m resolution Fire Island Strip grid (only a 15-km wide alongshore section near the 2014 Experiment platforms are shown). "x" in (a) and (b) indicates the location of the NDBC Buoy#44066; square in (b) indicates the location of the NDBC Buoy#44065; circle in (b) indicates the location of the NDBC Buoy#44025; triangle in (b) indicates the location of the NDBC Buoy#44017; dots in (c) and (d) indicate the locations of the platforms in the 2014 Experiment. Thin black curves in (b), (c), and (d) delineate the shoreline.

the nearshore sand bar morphology (section 3.3). The analysis showed that 82% of the alongshore sediment flux between the coast and 13.5 m depth is occurring between the coast and 8 m depth. The alongshore variations of the alongshore transports integrated between 0–8 m and 0–13.5 m are virtually identical (with a correlation coefficient of 0.99) and using either one does not change the findings presented here. Therefore, the fluxes integrated up to 13.8 m are used. Based on the surficial sediment samples obtained using a Van Veen-type grab sampler during the field experiments in the area in 2014, D_{50} was taken as 250 μm (Poppe et al., 2014) which is medium-fine sand.

Although we would have liked to simulate the entire period of shoreline observations, that was not feasible due to computational limitations, as well as lack of high-quality input data for winds and wave boundary conditions for the entire period. Therefore, we selected a manageable period of time for modeling, 1994–1999, in which we observed the shoreline shape going back to very close to the long-term mean shape (with the series of persistent shoreline features) from a period that it was not, meaning that the wave climate during this period is expected to be conducive to the generation of the long-term mean shape.

3.2. Model-Data Comparison

The quadruple-grid model setup is evaluated against both observations from an inner-shelf deployment and a long-term buoy data set. The deployment data set consists of a series of observations collected offshore of the western half of Fire Island. The experiment was conducted between February and May 2014 (Armstrong et al., 2015) to study nearshore processes along the western half of Fire Island to investigate modifications of currents and waves due to the presence of the offshore SFCR. Wave gauges and buoys were placed at six sites along the 12 m isobath about 1 km off the coast; two other sites were located offshore of this alongshore array at 14 and 16 m depths; and one offshore wave buoy was deployed at 26 m water depth 7 km offshore (Figures 1, 3c, and 3d). Two National Data Buoy Center (NDBC) buoys, #44066 at 82 m depth (39.584 N, 72.6 W) and #44017 at 52 m depth (40.694 N, 72.048 W), also provided wind and

wave data during the experiment. NDBC#44025 that was closest to the sites (40 m depth; 40.251 N, 73.164 W; see in the inset in Figure 1 and also the circle in Figure 3b) was not operating during this experiment, but provided historical wave observations that extend back to the 1990s (Figure 6). The locations of these NDBC buoys offshore are also shown in Figures 1 and 3. The nearshore sites between 12 and 16 m depth are all within the strip grid domain (dots in Figures 1, 2b, and 3d); the buoy deployed at 26 m depth is within the shelf grid domain (the dot offshore in Figures 3c and 3d); NDBC#44017 is within the New York Bight grid domain (triangle in Figure 3b); NDBC#44066 is within the USEast grid domain ("x" in Figures 3a and 3b). All the field observations detailed in this section, and the bathymetry data and model hindcasts mentioned above are open source and available online (detailed in Acknowledgments).

The model results were also evaluated using a longer-term data set that covers the modeled period between 1994 and 1999. This period was selected because it represents a duration which the persistent shoreline undulations progress from a less pronounced shape to a series of stronger shoreline features observed in the shoreline position data set (section 2). Historical observations at the NDBC#44025 buoy offshore of Fire Island were used for evaluating the model performance during this modeled period. The only available observations on nearshore sediment transport are the shoreline shape data (described in section 2) and the model results are also compared with those (section 4), in addition to these wave observations.

Model-data comparison for the 2014 experiment is shown in Figure 4. Significant wave height along the 12 m isobath exceeded 2 m at several storms when wind energy was relatively high with speeds reaching or exceeding 15 m/s. During these high-energy events, waves at the 26 m depth buoy were predominantly from East-South-East and South-South-East, consistent with the long-term wave climatology of the area (Figure 6). The model results compare well with the observations (Figure 4), although some peaks in the observed wave energy, such as those on 14 February, 8 March, and 30 April (with wave directions of 100–140° measured at 26 m depth), are underestimated by the model. On the other hand, the model slightly overestimates the wave energy in some other storms such as those on 13 March and 15 April (with wave directions of 170–300° measured at 26 m depth). Overall, the results indicate that the model is able to

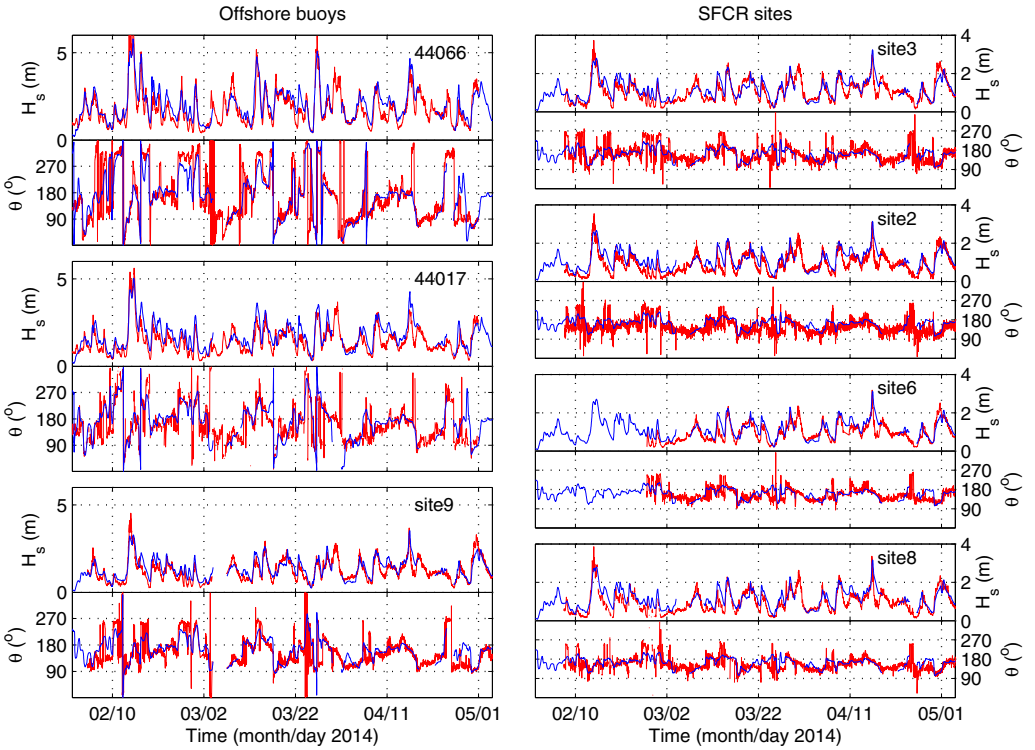

Figure 4. Model-data comparison during the 2014 Experiment. Model results are shown in blue; observations are shown in red. The left plot shows comparisons for offshore buoys NDBC#44066 (82 m depth), NDBC#44017 (52 m depth) and the deployed buoy at site 9 (26 m depth). The right plot shows comparisons from sites 3 (16 m depth), 2 (12 m depth), 6 (12 m depth), and 8 (12 m depth). Buoy and site locations are shown in Figures 1, 2, and 3.

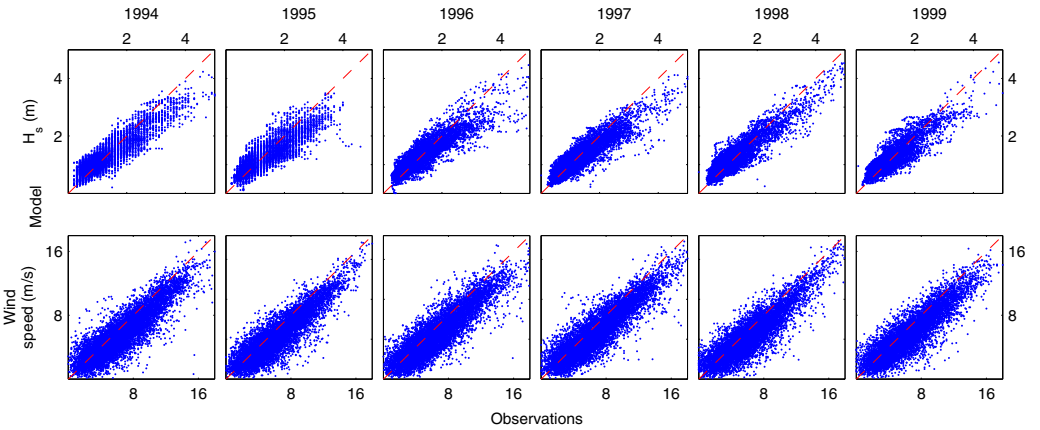

Figure 5. Model-data comparison of waves (top plots) and winds (bottom plots) at the NDBC#44025 buoy (40 m depth; circle in Figure 3b) between 1994 and 1999. Dashed red lines show the one-to-one relationships.

compute the temporal and spatial evolution of waves observed both across the inner continental shelf off Fire Island (starting from offshore at 82 m depth up to the 12 m isobath in the nearshore) and also along the SFCR field (sites that were located along the 12 m isobath).

Figure 5 shows the model-data comparison based on the historical long-term wave and wind observations at the NDBC#44025 buoy (40 m depth; circle in Figure 3b) during the 6 year modeling period between 1994 and 1999. The model results are in fair agreement with the observed waves with an average $r^2 = 0.79$. The model is underestimating the wave heights at some energetic events which can in part be attributed to imperfections related to the available wind hindcasts used as model forcing input which are also underestimating the observed wind speed at energetic events, albeit good correlation ($r^2 = 0.78$). To evaluate the wave climatology within this 6 year modeling period versus the 50 year period covering the shoreline position data set, wave observations from the NDBC Buoy#44025 are analyzed and waveroses are obtained (Figure 6). The waverose based on the observations from the entire record of this buoy (1991–2013; Figure 6a)

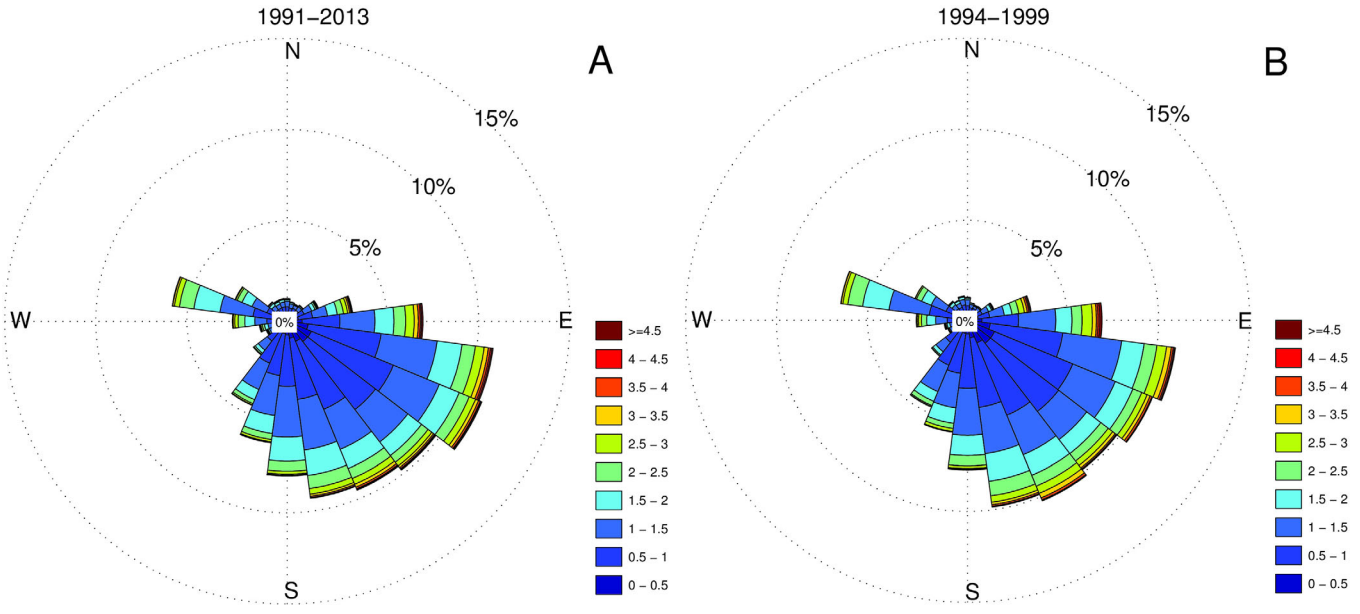

Figure 6. Waveroses based on the directional wave observations from the NDBC Buoy#44025 at 40 m depth offshore of Fire Island (indicated in the inset in Figure 1 and also by the circle in Figure 3b). Directions indicate where waves are coming from. Plots (a) and (b) show the waveroses based on the entire historical record from this buoy (1991–2013) and the 1994–1999 period modeled here, respectively.

and the one based on the observations within the 1994–1999 period modeled here (Figure 6b) are very similar. This suggests that the wave climatology within this modeled period represents the longer-term wave climatology at the study site.

3.3. Nearshore Straightening

The nearshore strip grid (Figure 3d) was generated to resolve nearshore flow processes and to test if the SFCR affect these processes. To investigate these processes, the nearshore bathymetry was smoothed using a moving averaging in order to remove the seasonal ephemeral features such as sand bars. Based on the examination of cross-shore bathymetry profiles, the 8 m isobath was determined to be at a location onshore of the SFCR field and also offshore of all the nearshore three-dimensional sand bar morphology. Therefore, smoothing was performed on the nearshore bathymetry between the coast and the 8 m isobath, gradually decreasing from the 6 m isobath to 8 m isobath where no smoothing is done so that the SFCR field is completely preserved in the bathymetry. Further details of the smoothing procedure are given by Safak et al. (2017).

We also hypothesize here that if the shoreline was straight in the region with SFCR offshore, the SFCR features would cause alongshore gradients of alongshore sediment transport within the nearshore region. On the other hand, transport gradients associated with variations in the shoreline and nearshore bathymetry with no SFCR offshore might have a smoothing effect on the coast (detailed below). Certainly, as the shoreline features evolve, they would feedback to their development. However, the simulations are done and the sediment fluxes are computed in a morphostatic sense here because accounting for morphological feedback along a 50 km-wide beach (spatial scales on the order of 10 km) over a 6 year-long time period (temporal scales of years) with a hydrodynamics-based model is extremely difficult both technically and numerically due to computational expense, uncertainties in long-term cross-shore transport modeling and development of numerical instabilities in these modeling systems, etc. In our case, although the long-term persistent undulations in the shoreline and nearshore contours might be induced by SFCR, we hypothesize that if the system is in quasi-equilibrium with the SFCR and these persistent undulations, the model predictions of alongshore sediment flux may include the effect of these undulations and may not be able to explain the formation of these persistent features. Therefore, in order to test our hypothesis that the generation of these persistent undulations on the shoreline is induced by the SFCR offshore, the nearshore bathymetry within the 15 km section of interest (km 6–21; section 2; Figure 2) is modified such that the shoreline is straightened by removing the undulations. The objective of this smoothing is to isolate the SFCR effects as the only bathymetric perturbation that acts on the sediment transport patterns.

The model setup and the nearshore straightening approach were first evaluated by computing the nearshore sediment fluxes for the 2014 Experiment (February–May 2014). Tests were done on two bathymetries. The first test (T1) was performed on the original available bathymetry which has both SFCR and persistent shoreline undulations as the influences on nearshore waves and sediment processes (Figure 7a). The second test (T2) was conducted on the bathymetry where the shoreline undulations are straightened to create a uniform, linear nearshore. This test has the SFCR as the bathymetric feature influencing on nearshore waves and sediment processes (Figure 7b). The SFCR are so irregularly distributed over the shelf offshore of the western half of the island (Figures 1 and 3c) with spatially varying shape, size, and depth range that filtering the SFCR from the large-scale shelf bathymetry is not possible. However, the difference between the two tests T1 and T2 removes all the SFCR and the shelf bathymetry by preserving the shoreline undulations and shows the effects of shoreline undulations on nearshore processes (Figures 7c and 7f). Figures 7d and 7e shows the net cross-shore integrated alongshore sediment fluxes for this 3 month period (converted to annual rates). The dominant energetic waves were from Southeast and driving a net westward sediment flux. The coastal straightening effect of having the shoreline undulations on the bathymetry is evident from the difference of the results from these two tests. The difference between the alongshore sediment flux estimates from these two bathymetries (T1–T2) is nearly a mirror image of the alongshore variation of alongshore sediment flux needed to generate the shoreline undulations, especially between km 7–17 (Figure 7f). Therefore, in order to test our hypothesis on the connection between the SFCR and the shoreline shape and to remove the coastal straightening effect due to the shoreline undulations themselves, the numerical simulations for 1994–1999 are conducted on the bathymetry with the straightened nearshore.

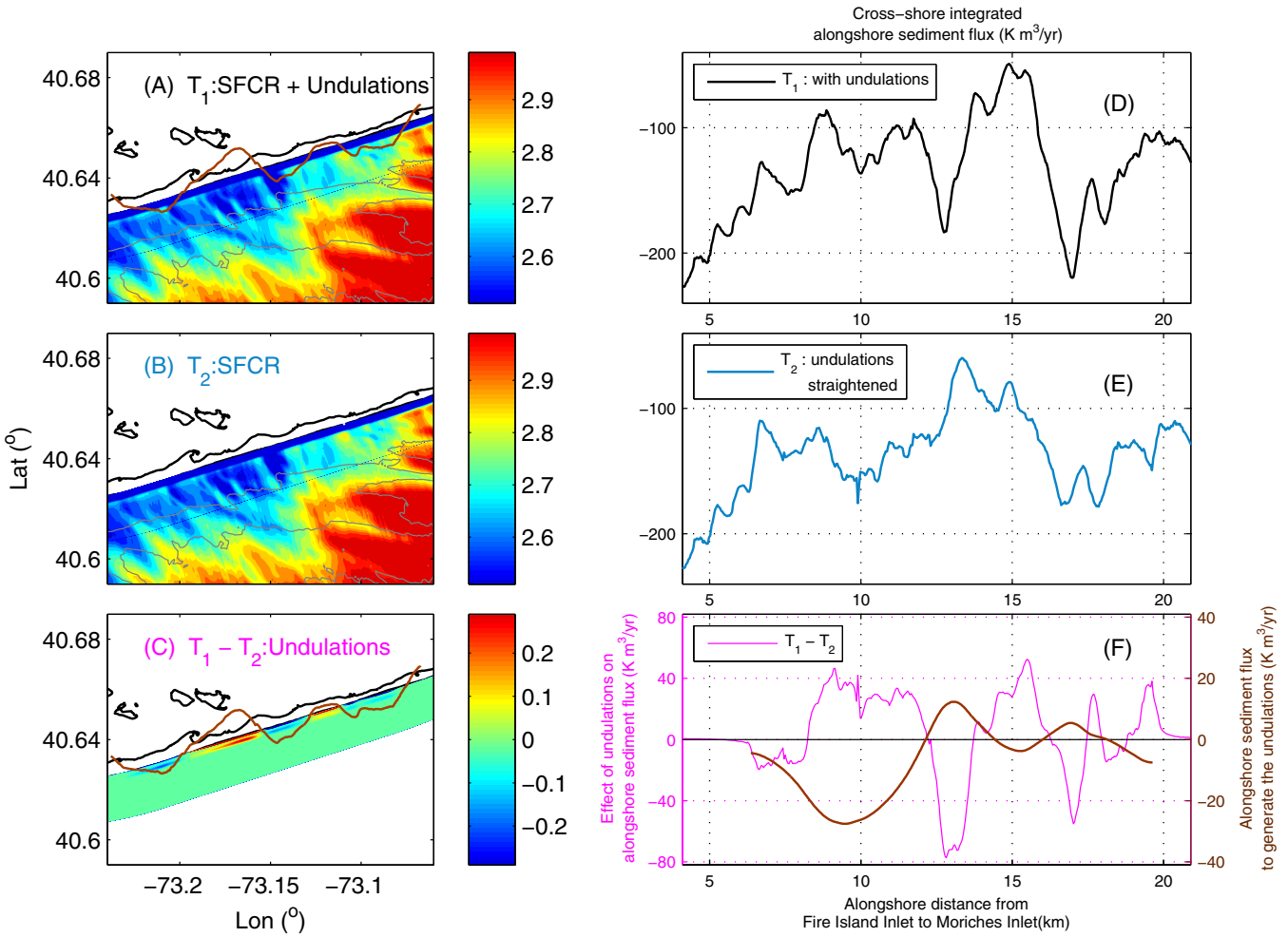

Figure 7. Coastal straightening effect of having the shoreline undulations on the bathymetry, tested for the February–May 2014 Experiment. Top, middle, and bottom plots correspond to the computations done on the bathymetry with SFCR and shoreline undulations (T1), computations done on the bathymetry with only SFCR (undulations straightened; (T2), and the difference between these two cases (T1–T2), respectively. Plots (d) and (e) show the net (February–May 2014) cross-shore integrated alongshore sediment flux computed in T1 and T2, respectively; plot (f) shows T1–T2. Left plot shows spatial variations of wave heights (in m) computed for 14 February 2014, 00:00 when energetic waves from Southeast drove westward sediment flux: (a) and (b) are significant wave heights computed on T1 and T2, respectively; (c) shows the difference between these two cases (in m). Black curves in (a), (b), and (c) delineate the shoreline; grey curves in (a) and (b) correspond to the 15, 20, and 25 m isobaths; brown curves in (a) and (c) delineate the persistent undulations on the shoreline exaggerated in the cross-shore direction.

4. Results

The coupled modeling system and the nested grid approach were used for simulating the waves and nearshore flows for the long-term period from 1994 to 1999. Results from these long-term simulations are shown in Figure 8 (from Fire Island Inlet at the west to Moriches Inlet at the east) as variation of cross-shore integrated alongshore sediment flux. Figure 8a shows the wave heights computed offshore of the persistent undulation zone. As expected, energetic wave events are correlated with greater magnitudes of sediment fluxes (Figures 8b and 8c). Figure 8 also reveals the interseasonal and interannual variability in sediment fluxes, such as: (i) relatively calm conditions in summer months and energetic conditions in winter and early spring; (ii) westward transport (negative values) dominating most of the years; (iii) 1997 appearing as a year with smaller westward transport and some significant eastward transport (positive values); and (iv) 1998 having relatively high westward fluxes.

Net alongshore sediment flux, time-averaged over this 6 year period of 1994–1999, is shown in Figure 9. Within the planar beach zone east of km-30 (Figure 1), alongshore sediment flux is mostly between −50 K and −100K m^3/yr (negative westward; Figure 9b). Into the western half of the island where the SFCR start

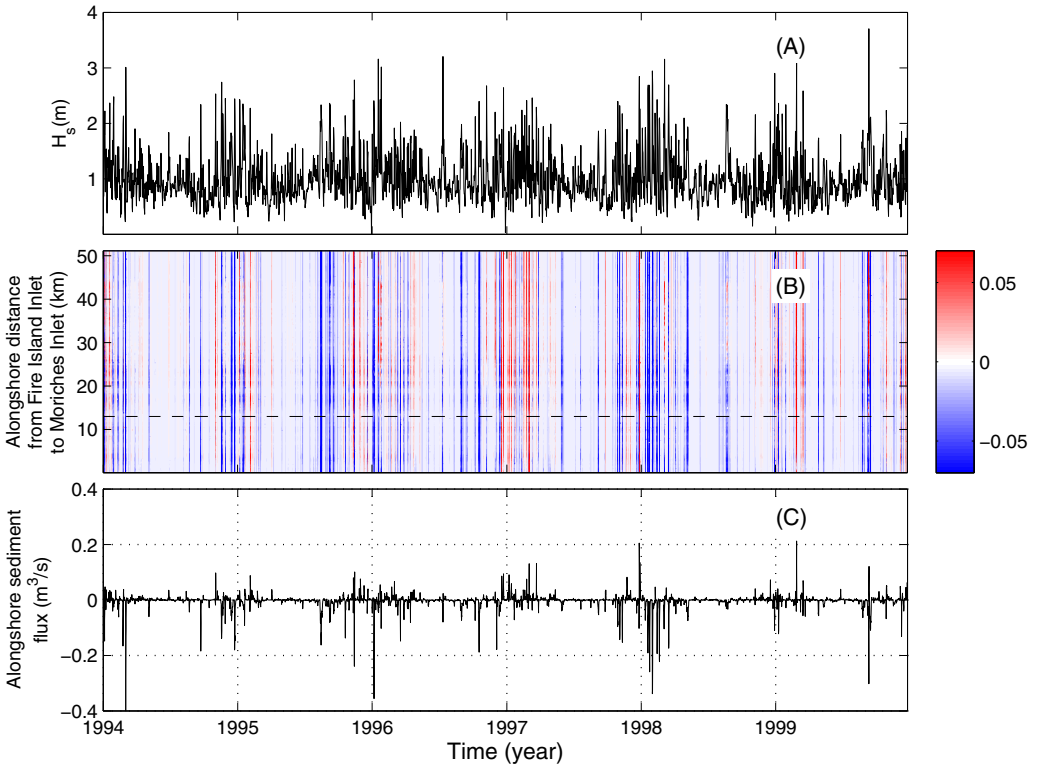

Figure 8. Summary of the wave conditions and alongshore sediment fluxes between 1994 and 1999: (a) Significant wave height at 16 m depth offshore of the middle of the persistent undulation zone (on the offshore boundary of the strip grid); (b) cross-shore integrated alongshore sediment flux (m^3/s) along the entire island; (c) cross-shore integrated alongshore sediment flux (m^3/s) at km-13 in the middle of the persistent undulation zone (location indicated with the dashed black line in plot (b). Negative indicates sediment flux toward the Fire Island Inlet, i.e., roughly westward; positive indicates sediment flux toward the Moriches Inlet, i.e., roughly eastward.

to dominate the inner-shelf bathymetry (Figure 1), an increasing trend in alongshore sediment flux is seen, first rapidly from km-30 to km-17 (Figure 9b). Variations of alongshore sediment flux are relatively large offshore of the persistent undulation zone, especially between km 10–16 where the persistence of the undulations is known to be high (section 2). From km-13 all the way to the Fire Island Inlet at the western end (km 0), there is again an overall increasing trend to rates around −200K m^3/yr, which is about 100K m^3/yr greater than those computed near the Moriches Inlet at the east. This net westward sediment flux along the island with an overall increasing trend from the Moriches Inlet at the east to the Fire Island Inlet at the west, and annual transport rates on the order of 100 K m^3/yr with rates past near Fire Island Inlet being on the order of 100 K m^3/yr greater than rates past Moriches Inlet are consistent with previous estimates for Fire Island (Kana et al., 2011; Rosati et al., 1999; Schwab et al., 2013). This increase in westward sediment flux from east to west, evident in all the studied years (Figure 9c), could partly be attributed to the dominant Southeast waves reaching at the western half of the island more obliquely (near Fire Island Inlet, shoreline orientation is about 5° counterclockwise from East; Figure 1) than they reach at the eastern end (near Moriches Inlet, shoreline orientation is about 25° counterclockwise from East).

Alongshore sediment fluxes computed on the bathymetry with the straightened nearshore compare well with the sediment flux required to generate the observed promontories and embayment between km 7–15.5 (Figures 10a and 10b). The sediment convergence zones (decreasing westward transport) between km 7–9.5 and km 13–15.5 (promontories), and the sediment divergence zone (increasing westward transport) between km 9.5–13 (embayment) are all well captured by the model. These results show that the sediment fluxes computed using the model are such that they would promote the observed promontories and embayment between km 7–15.5. However, the modeled patterns between km 15.5–18 do not compare that well with the observations. Offshore of this part of the persistent undulation zone is where the two major dredging areas on SFCR are located (Figure 1). That region is also recently documented to be

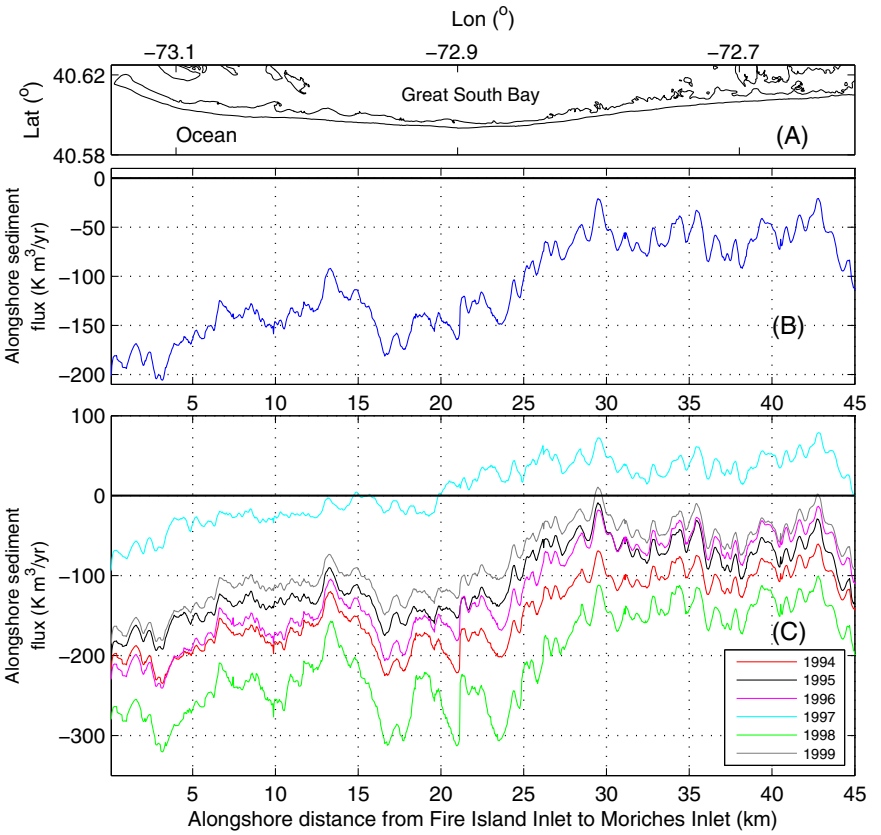

Figure 9. Model estimates of alongshore sediment fluxes: (a) Shoreline, slightly tilted to align with the approximate alongshore direction; (b) Alongshore variation of cross-shore integrated net annual alongshore sediment flux rate (averaged over the 1994–1999 period); (c) Alongshore variation of cross-shore integrated net annual alongshore sediment flux rate for each year between 1994 and 1999.

relatively dynamic in terms of changes in bathymetry and sediment thickness (Schwab et al., 2016). These observations reveal that the effects of bathymetric variability in this area could be high. Interestingly, also the persistence of the shoreline undulations is smaller between km 16–20, compared to km 7–16 (section 2). In addition, the coastal straightening effect of having the shoreline undulations in the km 16–20 section is not as obvious as the one for the undulations in km 7–16 (section 3.3; Figure 7f). Therefore, the model computations tend to generate the observed shoreline features with similar scales within the high-persistence section of the persistent undulation zone (highlighted with dark brown in Figures 2b and 10a). This is the case after the undulations are removed from the nearshore bathymetry by straightening the shoreline and the only bathymetry-induced variation left is due to SFCR offshore.

One way to compare the model results and the observations is to look at the "sediment flux residual" (section 2), i.e., what is left from the modeled alongshore sediment transport after the effect of sediment flux needed to generate the shoreline undulations (shoreline-derived transport) is removed (Figure 10c). This sediment flux residual fluctuates around zero and is relatively small in the zone from km 7–15 which means that the modeled alongshore sediment fluxes explain fairly well the generation of the persistent shoreline undulations in this zone. In particular, the model explains the existence of the most prominent shoreline embayment, centered at 12 km. The sediment flux residual has its most significant values in the zone of discrepancy between km 15–17 where it shows that modeled alongshore transport gradients are producing excess sediment (Figure 10c). To investigate this discrepancy between the modeled alongshore sediment fluxes and the sediment flux needed to generate the observed persistent shoreline undulations (Figure 10b), near-bed cross-shore flows between the inner continental shelf and the nearshore are analyzed. Mean cross-shore velocities averaged over the 6 year period between 1994 and 1999 are shown in Figure 10d. Offshore of the persistent undulation zone between km-15 and

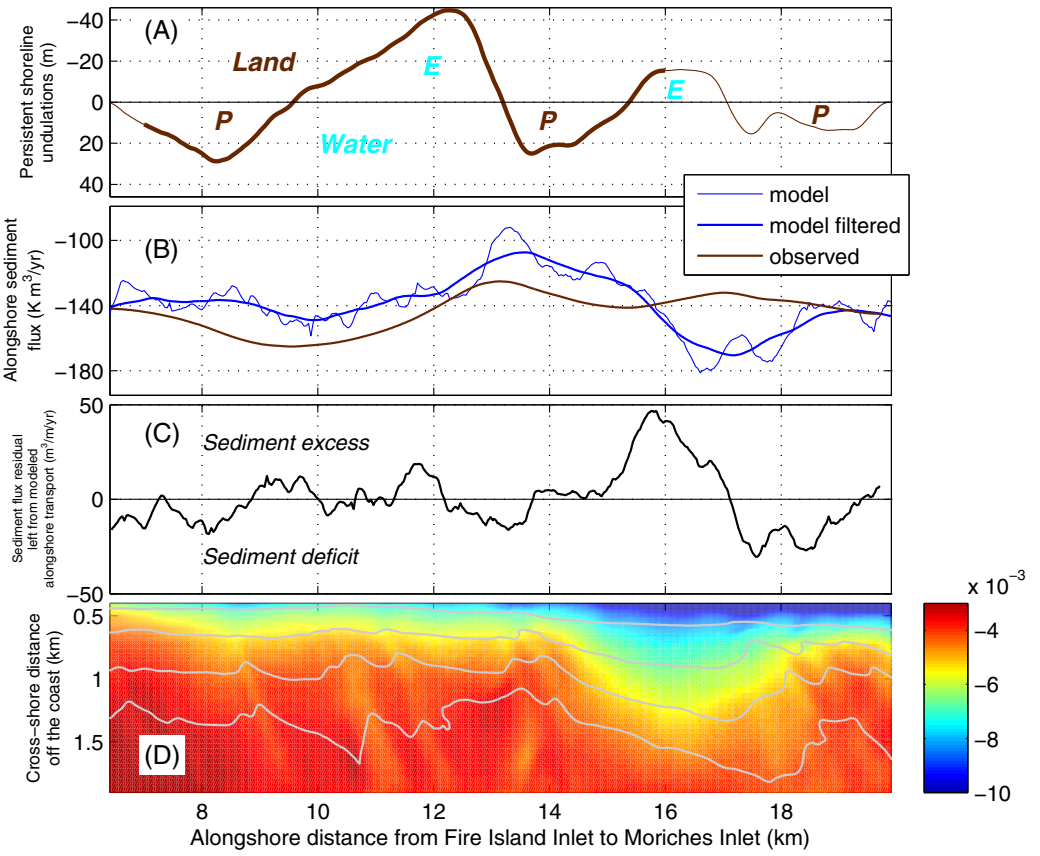

Figure 10. Alongshore variation of: (a) persistent shoreline undulation (Figure 2) shape (positive and negative values indicate promontory "P" and embayment "E," respectively; darker brown highlights the part of the section where the persistence is higher); (b) cross-shore integrated alongshore sediment flux estimated by the model (averaged over 1994–1999; thin blue), filtered estimate of the model (thick blue), and alongshore sediment flux needed to generate the observed persistent shoreline undulation shape (brown); (c) sediment flux residual left from explaining the persistent shoreline undulation shape only by modeled alongshore transport (positive values indicate that the modeled alongshore transport is producing excess sediment compared to the one needed to generate the observed persistent shoreline undulation shape); (d) cross-shore velocities near bed, averaged over 1994–1999 (m/s; negative values indicate offshore flow; gray curves correspond to the 8, 10, 12, and 14 m isobaths).

km-18 includes a prominent ridge crest (gray curves in Figure 10d indicate the 8, 10, 12, and 14 m isobaths) and is a distinct region in the alongshore variation of the cross-shore velocities. Within this region, cross-shore velocities near the bed are distinctly more offshore (Figure 10d), possibly due to offshore deflection of the westward wind- and wave-driven currents which are dominant along Fire Island (Warner et al., 2014). This could contribute to a less convergent (less accretionary) and more erosive sediment flux pattern. It is encouraging that the cross-shore flows are showing a stronger offshore pattern that could explain part of the model-data discrepancy in this area where modeled alongshore sediment fluxes predict a convergence zone (formation of a promontory; Figure 10b) but the observations show a relative embayment (Figure 10a).

5. Discussion

In this section, further investigation of the results for individual years shows interesting interannual variability of sediment fluxes and provides more explanation of the physical processes driving these fluxes. This is followed by additional discussion of the results based on the findings from previous related studies, and then the diagnostic analysis of the physical processes in the nearshore that promote the generation of the persistent shoreline undulations.

5.1. Interannual Variability of Transport

The cross-shore integrated (section 2) alongshore sediment fluxes for all the modeled years show similar trends of transport increasing westward from Moriches Inlet to Fire Island Inlet (Figure 9c). Of all the years simulated, the highest net sediment fluxes occurred in 1998. This year also showed the most variability of alongshore sediment flux, especially in the area of the persistent undulation zone. During one of the years, 1997, there was significant eastward transport (Figure 9c). To investigate this anomalous trend, wave climatologies for the years between 1994 and 1999 were compared. It was identified that the year 1997 was a year with relatively high wave forcing from Southwest and less energetic storms from the Southeast, the typical dominant wave direction at the study site (Figures 11a and 11b). The interesting aspect of the year 1997 related to the persistent shoreline undulations is that the alongshore variations of sediment fluxes modeled for that year are notably different than those for the 1994–1999 period (Figure 11c). The modeled alongshore sediment fluxes for 1997 show an almost opposite pattern of the sediment flux needed to generate the observed shoreline undulations (Figure 11c). This is consistent with the findings of the wave refraction analysis from Xu et al. (2016). They performed numerical simulations on an idealized set of SFCR, varied the wave forcing magnitudes and directions, and revealed that: (i) SFCR can trap more wave energy when waves approach with an angle close to ridge orientation (i.e., propagation along SFCR) as compared to when waves approach perpendicular to ridge crests (i.e., propagation across SFCR), and (ii) these differences in wave directionality result with opposite patterns in corresponding alongshore gradients of transport.

5.2. Shoreline Observations of Allen and LaBash (1997)

Here, we attempt to explain the long-term persistent shape of the shoreline onshore of the SFCR. Accordingly, it is worth considering the shoreline change observation of Allen and LaBash (1997), which motivated the initial hypothesis that the offshore ridges and troughs exert control on the shoreline response (Schwab

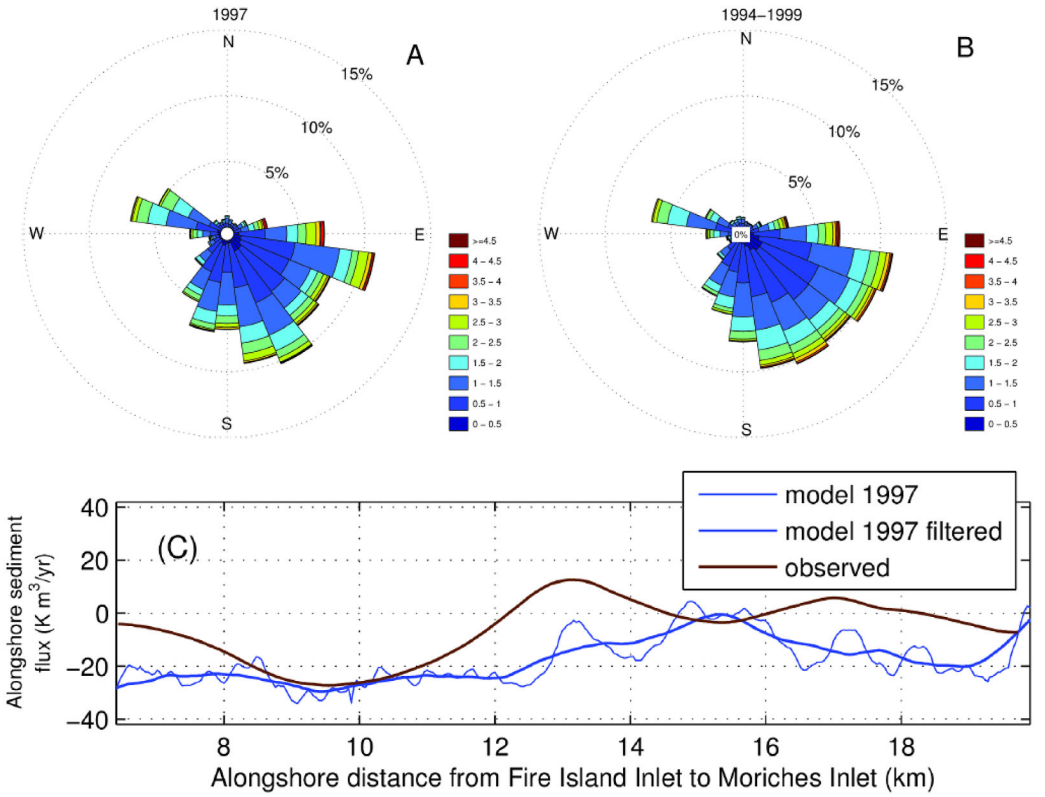

Figure 11. Waveroses based on the directional wave observations from the NDBC Buoy#44025 (a) for 1997; (b) for the 1994–1999 period. (c) Alongshore variation of cross-shore integrated alongshore sediment flux estimated by the model for 1997 (thin blue), filtered estimate of the model (thick blue), and alongshore sediment flux needed to generate the observed persistent shoreline undulation shape (brown).

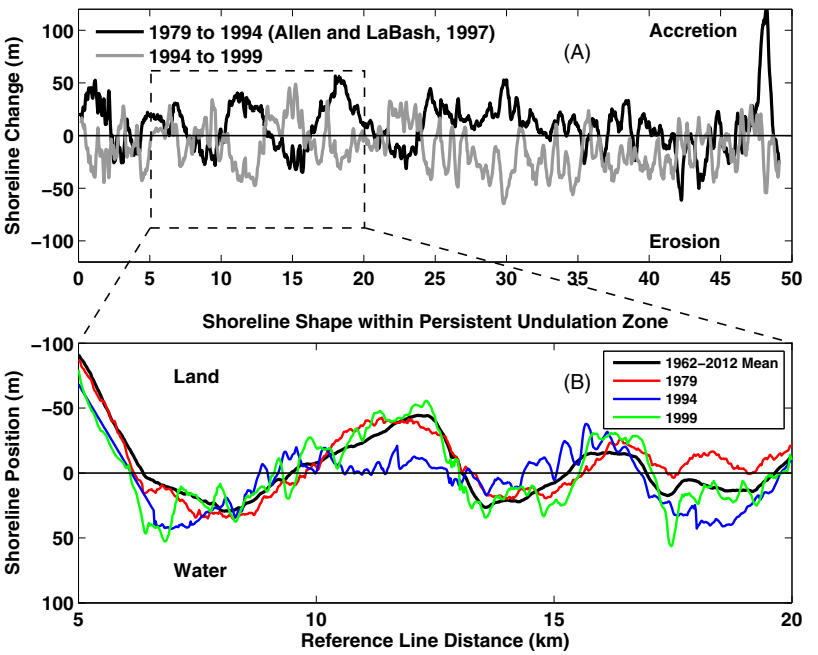

Figure 12. (a) Reproduction of the 1979–1994 shoreline change observation of Allen and LaBash (1997), with the 1994–1999 shoreline change added for comparison; (b) shoreline position within the persistent undulation zone.

et al., 2000). Within the persistent undulation zone (km 6–20), the 1979–1994 shoreline change result of Allen and LaBash (1997), reproduced in Figure 12a, shows a distinct mirror-image pattern relative to 1994–1999 shoreline change. Shoreline positions for 1979, 1994, and 1999 (Figure 12b) show that shoreline change can be explained by individual shorelines that follow more, or less, of the long-term average shape, and that deviations from the long-term average shape in the 1994 shoreline are subsequently reversed by 1999. Our interpretation is that deviations from a wave climate that supports the maintenance of the persistent shoreline undulations, such as we have seen in the 1997 model results (Figure 11), could explain periods when the shoreline shape differs from the long-term average shape. However, as seen in Figure 2, the vast majority of shorelines surveyed between 1962 and 2012 exhibit some degree of the persistent shoreline shape.

5.3. Diagnostic Analysis of Transport

For an in-depth investigation of the nearshore processes that generate the persistent undulations on the shoreline, a storm with an alongshore sediment flux pattern that has the highest correlation with the long-term sediment flux patterns is selected. This storm occurred on 27 January, 1996 when waves with 3 m significant wave height and 10 s period were propagating to Fire Island from Southeast, and a diagnostic momentum balance analysis is conducted. The momentum terms are analyzed to isolate the effects of the SFCR on the nearshore without including the momentum on the SFCR themselves. To accomplish this, the terms in the alongshore momentum balance (equation (3)) are integrated in the cross-shore starting from the coast up to 8 m depth which is onshore of the SFCR field (section 3.3) and are shown in Figure 13. Energetic waves from Southeast drive a negative wave breaking term (toward west; Figure 13b) which is the dominant driving term of the alongshore momentum balance and the resulting alongshore flow and sediment fluxes. The SFCR control (i) how waves refract, (ii) how waves have their alongshore wave power reduced (Figure 13a) and, therefore, (iii) the variation of the alongshore wave breaking term (Figure 13b). This is the most evident for the prominent ridge crest between km 14–17 which causes offshore waves to start to refract relatively far from the coast and reduces their alongshore wave power (Figure 13a) and, therefore, reduces also the alongshore wave breaking term in that region (Figure 13b). These reveal the connection between the geometry of the SFCR, the alongshore variation of the sediment fluxes and the resulting positions of the promontories and the embayments on the shoreline undulations. The main term that balances wave breaking is the bottom stress. Horizontal advection and vortex force terms (Kumar et al.,

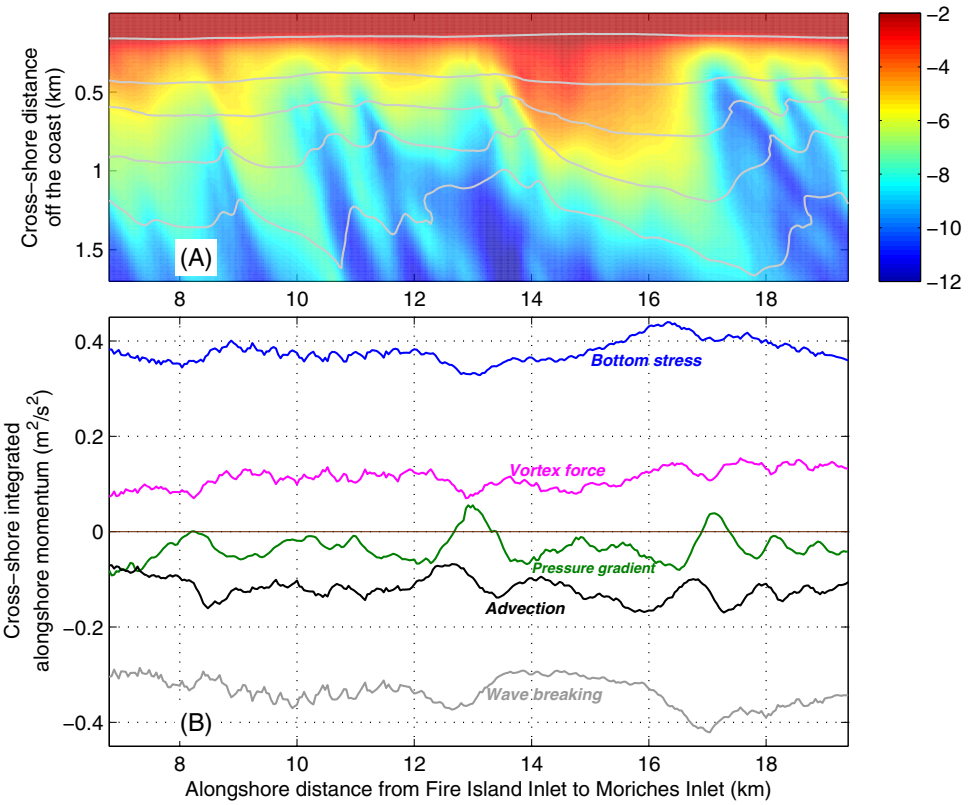

Figure 13. Alongshore variation of: (a) Alongshore wave power (in KWatts/m) offshore of the persistent shoreline undulation zone (negative values indicate that waves are propagating westward in the alongshore; gray curves correspond to 4, 8, 10, 12, and 14 m isobaths); (b) Cross-shore integrated alongshore momentum balance terms: wave breaking (gray), bottom stress (blue), pressure gradient (green), horizontal advection (black), and vortex force (magenta).

2012) tend to balance each other. The pressure gradient is negative and drives the flow to the west, except for onshore of the two most prominent ridge troughs. At these locations the velocities are increasing and so the pressure gradient is decreasing to balance the flows. This analysis shows that the important processes driving the alongshore flows and sediment fluxes in the nearshore during this representative storm are wave breaking, vortex force, horizontal advection and pressure gradient, all of which are influenced by the SFCR effects on nearshore processes.

6. Conclusions

In this study, inner-shelf geologic framework was shown to have a strong influence on the adjacent shoreline shape. We tested the hypothesis that the generation of large-scale persistent undulations at the shoreline is linked to the effects of shoreface-connected sand ridges (SFCR) on nearshore wave and sediment processes. Fire Island, New York was selected as the study site and the reasons are twofold: SFCR dominates the inner-shelf offshore of the western half of Fire Island, and the shoreline position observations along this island covering the last 50 years indicate in this western half a 15 km long persistent shoreline undulation shape with cross-shore amplitudes of 20–40 m and an alongshore wavelength on the order of 1 km. To investigate our hypothesis, a three-dimensional hydrodynamics-based model was setup and first tested with observations at depths between 82 m and 12 m depth during a large-scale field experiment in 2014, and also using the historical measurements from the nearby buoys. Model results here are consistent with recent studies and indirect observations in the area, showing net westward alongshore sediment flux on the order of 100 K m^3/yr, with the island characterized in three segments: an eastern region with transport rates between 50 K and 100 K m^3/yr, a central region of increasing transport, and the western region where the shoreline undulations are observed, with transport rates twice as big as those in the eastern region. In terms of interannual variability, a year with relatively high wave forcing from South and Southwest was

found to be associated with alongshore sediment fluxes that are smaller and in parts in the opposite direction of the predicted long-term mean direction of transport. The model predicted the generation of the high-persistence undulations at the shoreline when the only bathymetric effect is caused by the SFCR field after these undulations on the nearshore bathymetry are straightened, which supports our hypothesis. The alongshore scale of the persistent shoreline undulations was well predicted by the model; the positions of relative embayments and promontories were also predicted accurately in one area but not in another. In this latter part of the persistent undulation zone, where alongshore sediment fluxes predict a promontory formation but the observations show a relative embayment, offshore currents from the nearshore toward the inner continental shelf were distinctly stronger than those in the adjacent areas. This qualitatively suggests that the cross-shore flows between the inner continental shelf and the nearshore are important in coastal evolution and the decadal scale shoreline shape. Diagnostic analysis of a representative storm reveals the effects of SFCR on wave refraction and wave power, and a resulting alongshore momentum balance between wave breaking, bottom stress, vortex force, horizontal advection, and pressure gradient. This shows that the sediment fluxes and shoreline shape are being controlled by the effects of offshore geologic framework on physical processes in the nearshore region.

Acknowledgments

This study was supported by the United States Geological Survey Coastal Change Processes Project. The first author was supported by a United States Geological Survey Mendenhall Research Fellowship. The authors acknowledge Wayne E. Baldwin for compilation of a major part of the bathymetry data, Field Support Group of the USGS-WHSC for the experimental data, Maria Liste, Erika Lentz, Kevin Haas, Tongtong Xu, Shawn Harrison and Tarandeep Kalra for fruitful discussions, the Editor Dr. Robert Hetland, the Associate Editor, and the two anonymous reviewers for their suggestions toward improving the manuscript. All the observations and model hindcasts used in this study are open source and available online: The shelf bathymetry data set can be accessed from https://pubs.usgs.gov/of/2014/1203/. The 2014 field experiment data set can be accessed from https://pubs.usgs.gov/of/2015/1033/. The data sets from the NOAA buoys can be accessed from http://www.ndbc.noaa.gov/, using the buoy numbers. Wave hindcasts of the WaveWatch III model were downloaded from the repository at http://polar.ncep.noaa.gov/waves/. Wind hindcasts of North American Regional Reanalysis (NARR) were downloaded from ftp://ftp.cdc.noaa.gov/Datasets/NARR/monolevel/. Any use of trade, product, or firm names is for descriptive purposes only and does not imply endorsement by the U.S. Government.

References

Allen, J. R., & LaBash, C. (1997). Measuring shoreline change on Fire Island. *Maritimes*, *39*, 13–16.

Armstrong, B. N., Warner, J. C., List, J. H., Martini, M. A., Montgomery, E. T., Traykovski, P., & Voulgaris, G. (2015). *Coastal Change Processes Project data report for oceanographic observations near Fire Island, New York, February through May 2014* (U.S. Geol. Surv. Open-File Rep. 2015–1033). Reston, VA: U.S. Geological Survey. https://doi.org/10.3133/ofr20151033

Ashton, A., Murray, A. B., & Arnault, O. (2001). Formation of coastline features by large-scale instabilities induced by high-angle waves. *Nature*, *414*, 296–300.

Chawla, A., Spindler, D. M., & Tolman, H. L. (2013). Validation of a thirty year wave hindcast using the Climate Forecast System Reanalysis winds. *Ocean Modelling*, *70*, 189–206. https://doi.org/10.1016/j.ocemod.2012.07.005

Denny, J. F., Schwab, W. C., Baldwin, W. E., Barnhardt, W. A., Gayes, P. T., Morton, R. A., . . . Voulgaris, G. (2013). Holocene sediment distribution on the inner continental shelf of northeastern South Carolina: Implications for the regional sediment budget and long-term shoreline response. *Continental Shelf Research*, *56*, 56–70.

Falques, A., Ribas, F., Idier, D., & Arriaga, J. (2017). Formation mechanisms for self-organized kilometer-scale shoreline sand waves. *Journal of Geophysical Research: Earth Surface*, *122*, 1121–1138. https://doi.org/10.1002/2016JF003964

Finkl, C. W., Benedet, L., Andrews, J. L., Suthard, B., & Locker, S. D. (2007). Sediment ridges on the West Florida inner continental shelf: Sand resources for beach nourishment. *Journal of Coastal Research*, *23*, 143–159.

Flocks, J. G., Kindinger, J. L., & Kelso, K. W. (2015). Geologic control on the evolution of the inner shelf morphology offshore of the Mississippi barrier islands, northern Gulf of Mexico, USA. *Continental Shelf Research*, *101*, 59–70.

Goff, J. A., Flood, R. D., Austin, J. A., Jr., Schwab, W. C., Christensen, B., Browne, C. M., . . . Baldwin, W. E. (2015). The impact of Hurricane Sandy on the shoreface and inner shelf of Fire Island, New York: Large bedform migration but limited erosion. *Continental Shelf Research*, *98*, 13–25.

Hapke, C. J., Lentz, E. E., Gayes, P. T., McCoy, C. A., Hehre, R., Schwab, W. C., & Williams, S. J. (2010). A review of sediment budget imbalances along Fire Island, New York: Can nearshore geologic framework and patterns of shoreline change explain the deficit? *Journal of Coastal Research*, *26*, 510–522.

Houser, C., Hapke, C., & Hamilton, S. (2008). Controls on coastal dune morphology, shoreline erosion and barrier island response to extreme storms. *Geomorphology*, *100*, 223–240.

Kaergaard, K., Fredsoe, J., & Knudsen, S. B. (2012). Coastline undulations on the West Coast of Denmark: Offshore extent, relation to breaker bars and transported sediment volume. *Coastal Engineering*, *60*, 109–122.

Kana, T. W., Rosati, J. D., & Traynum, S. B. (2011). Lack of evidence for onshore sediment transport from deep water at decadal time scales: Fire Island, New York. *Journal of Coastal Research*, *SI59*, 61–75.

Kumar, N., Voulgaris, G., Warner, J. C., & Olabarrieta, M. (2012). Implementation of the vortex force formalism in the coupled ocean-atmosphere-wave-sediment transport (COAWST) modeling system for inner shelf and surf zone applications. *Ocean Modelling*, *47*, 65–95.

Lentz, E. E., Hapke, C. J., Stockdon, H. F., & Hehre, R. E. (2013). Improving understanding of near-term barrier island evolution through multi-decadal assessment of morphologic change. *Marine Geology*, *337*, 125–139.

List, J. H., Safak, I., Warner, J. C., Schwab, W. C., & Hapke, C. (2016). Understanding long-term, large-scale shoreline change and the sediment budget on Fire Island, NY, using a 3D hydrodynamics-based model. *Abstract presented at 2016 Ocean Sciences Meeting*, New Orleans, LA: American Geophysical Union.

Liste, M., Warner, J. C., List, J. H., Safak, I., & Schwab, W. C. (2016). Hydrodynamics and sediment transport along and across shoreface-connected ridges: Fire Island, NY. *Abstract presented at 2016 Ocean Sciences Meeting*, New Orleans, LA: American Geophysical Union.

Pendleton, E. A., Brothers, L. L., Thieler, E. R., Danforth, W. W., & Parker, C. E. (2015). *National Oceanic and Atmospheric Administration hydrographic survey data used in a U.S. Geological Survey regional geologic framework study along the Delmarva Peninsula* (U.S. Geol. Surv. Open-File Rep. 2014-1262, 18 p.). Reston, VA: U.S. Geological Survey. https://doi.org/10.3133/ofr20141262

Poppe, L. J., McMullen, K. Y., Williams, S. J., & Paskevich, V. F. (2014). *USGS east-coast sediment analysis: Procedures, database, and GIS data* (U.S. Geol. Surv. Open-File Rep. 2005-1001). Reston, VA: U.S. Geological Survey. Retrieved from http://pubs.usgs.gov/of/2005/1001/; http://coastalmap.marine.usgs.gov/FlexWeb/national/usseabed/

Riggs, S. R., Cleary, W. J., & Snyder, S. W. (1995). Influence of inherited geologic framework on barrier shoreface morphology and dynamics. *Marine Geology*, *126*, 213–234.

Rosati, J. D., Gravens, M. B., & Smith, W. G. (1999). Regional sediment budget for Fire Island to Montauk Point, New York, USA. In *Proceedings of Coastal Sediments'99* (pp. 802–817). New York, NY: American Society of Civil Engineers.

Ruggiero, P., & List, J. H. (2009). Improving accuracy and statisical reliability of shoreline position and change rate estimates. *Journal of Coastal Research*, *25*, 1069–1081.

Safak, I., List, J. H., Warner, J. C., & Kumar, N. (2017). Observations and 3D hydrodynamics-based modeling of decadal-scale shoreline change along the Outer Banks, North Carolina. *Coastal Engineering*, *120*, 78–92. https://doi.org/10.1016/j.coastaleng.2016.11.014

Safak, I., Warner, J. C., & List, J. H. (2016). Barrier island breach evolution: Alongshore transport and bay-ocean pressure gradient interactions. *Journal of Geophysical Research: Oceans*, *121*, 8720–8730. https://doi.org/10.1002/2016JC012029

Schupp, C. A., McNinch, J. E., & List, J. H. (2006). Nearshore shore-oblique bars, gravel outcrops, and their correlation to shoreline change. *Marine Geology*, *233*, 63–79.

Schwab, W. C., Baldwin, W. E., & Denny, J. F. (2016). Assessing the impact of Hurricanes Irene and Sandy on the morphology and modern sediment thickness on the inner continental shelf offshore of Fire Island, New York (U.S. Geol. Surv. Open-File Rep. 2015–1238, 15 p.). Reston, VA: U.S. Geological Survey. https://doi.org/10.3133/ofr20151238

Schwab, W. C., Baldwin, W. E., Denny, J. F., Hapke, C. J., Gayes, P. T., List, J. H., & Warner, J. C. (2014). Modification of the Quaternary stratigraphic framework of the inner-continental shelf by Holocene marine transgression: An example offshore of Fire Island, New York. *Marine Geology*, *355*, 346–360.

Schwab, W. C., Baldwin, W. E., Hapke, C. J., Lentz, E. E., Gayes, P. T., Denny, J. F., . . . Warner, J. C. (2013). Geologic evidence for onshore sediment transport from the inner continental shelf: Fire Island, New York. *Journal of Coastal Research*, *29*, 526–544.

Schwab, W. C., Baldwin, W. E., Warner, J. C., List, J. H., Denny, J. F., Liste, M., & Safak, I. (2017). Change in morphology and modern sediment thickness on the inner continental shelf offshore of Fire Island, New York between 2011 and 2014: Analysis of hurricane impact. *Marine Geology*. *391*, 48–64. https://doi.org/10.1016/j.margeo.2017.07.010

Schwab, W. C., Thieler, E. R., Allen, J. R., Foster, D. S., Swift, B. A., & Denny, J. F. (2000). Influence of inner-continental shelf geologic framework on the evolution and behavior of the barrier-island system between Fire Island Inlet and Shinnecock Inlet, Long Island, New York. *Journal of Coastal Research*, *16*, 408–422.

Swift, D. J. P., Niederoda, A. W., Vincent, C. E., & Hopkins, T. S. (1985). Barrier island evolution, Middle Atlantic Shelf, USA. Part 1: Shoreface dynamics. *Marine Geology*, *63*, 331–361.

Warner, J. C., Armstrong, B., He, R., & Zambon, J. B. (2010). Development of a coupled ocean-atmosphere-wave-sediment transport (COAWST) modeling system. *Ocean Modelling*, *35*, 230–244.

Warner, J. C., List, J. H., Schwab, W. C., Voulgaris, G., Armstrong, B., & Marshall, N. (2014). Inner-shelf circulation and sediment dynamics on a series of shoreface-connected ridges offshore of Fire Island, NY. *Ocean Dynamics*, *64*, 1767–1781.

Warner, J. C., Perlin, N., & Skyllingstad, E. (2008b). Using the Model Coupling Toolkit to couple earth system models. *Environmental Modelling & Software*, *23*, 1240–1249.

Warner, J. C., Schwab, W. C., List, J. H., Safak, I., Liste, M., & Baldwin, W. (2017). Inner-shelf ocean dynamics and seafloor morphologic changes during Hurricane Sandy. *Continental Shelf Research*, *138*, 1–18.

Warner, J. C., Sherwood, C. R., Signell, R. P., Harris, C. K., & Arango, H. G. (2008a). Development of a three-dimensional, regional, coupled wave, current, and sediment-transport model. *Computers & Geosciences*, *34*, 1284–1306.

Wright, L. D., Boon, J. D., Kim, S. C., & List, J. H. (1991). Modes of cross-shore sediment transport on the shoreface of the Middle Atlantic Bight. *Marine Geology*, *96*, 19–51.

Xu, T., Haas, K., List, J. H., & Safak, I. (2016). Wave transformation and sediment transport over obliquely-oriented shoreface-connected ridges. *Abstract presented at 2016 Ocean Sciences Meeting*, New Orleans, LA: American Geophysical Union.